Current Optics and Photonics
Vol. 3, No. 5, October 2019, pp. 429-437

ISSN: 2508-7266(Print) / ISSN: 2508-7274(Online)
DOI: https://doi.org/10.3807/COPP.2019.3.5.429

Athermalization of an Optical System Based on Lens Shape and Assembly Method

Sihua Xu[1,2,3], Xiaoqiang Peng[1,2,3]*, Guipeng Tie[1,2,3], Chaoliang Guan[1,2,3], Hao Hu[1,2,3], and Yupeng Xiong[1,2,3]

[1]*Laboratory of Science and Technology on Integrated Logistics Support, National University of Defense Technology, Changsha 410073, China*
[2]*College of Intelligent Science, National University of Defense Technology, Changsha 410073, China*
[3]*Hu'nan Key Laboratory of Ultra-precision Machining Technology, Changsha 410073, China*

(Received July 11, 2019 : revised August 13, 2019 : accepted August 17, 2019)

Temperature adaptability is an important metric for evaluating the performance of an optical system. The temperature characteristics of the optical system are closely related to the material and shape of its lens. In this paper, we establish a mathematical model relating the temperature characteristics to the shape and material of the lens. Then a novel assembly structure that can solve the lens constraint and positioning problem is proposed. From those basics, the correctness of the theoretical model and the effectiveness of the assembly structure are verified through simulated analysis of the imaging quality of the optical system, whose operating temperature range is -60~100°C.

Keywords : Optical system, Athermalization, Temperature characteristics of focus, Thermal deformation, Assembly structure
OCIS codes : (120.4820) Optical systems; (120.4570) Optical design of instruments; (120.6810) Thermal effects

I. INTRODUCTION

Aerospace optical systems should have good temperature adaptability. If such an optical system does not have this property and does not operate at the designed temperature, the imaging quality of the system will be affected by temperature fluctuations [1]. The influence of temperature change on an optical system is mainly reflected in the geometric parameters of the optical components: the mirror spacings and the refractive index of the lens [2]. Many researchers have carried out valuable work about raising the temperature adaptability of optical systems. Vukobratovich found that there is no thermal aberration in a homogeneous material reflection system [3]. However, catadioptric optical systems are widely used, in which the primary and secondary mirrors are generally of homogenous material, and the subsequent optical components are generally lenses of different materials [4]. Therefore, there is value in researching the relationship between the temperature characteristics and the shapes and materials of the lens. The method of optical passive athermalization, which utilizes the thermal characteristics of optical components to achieve athermalization, is closely related to the material properties of the components. For example, Li used this method to design a compact medium-wave infrared imaging system with athermalization [5], and Kucukkacel designed a dual-field-of-view infrared optical system with good imaging quality in the temperature range of -40~60°C [6]. However, all of the above studies were limited to selection of lens materials; the influence of lens shape has not received sufficient attention [7-9]. To address this issue, researchers such as J. W. Perry proposed the concept of athermal design [10], by which the mechanical passive, mechanical active, and optical passive athermal methods are developed. The passive mechanical compensation technique and the active electromechanical athermal compensation technique are also mainly used to adjust the axial positions of optical elements [11]. However, due to the inconsistent thermal expansivity between optical-

*Corresponding author: pengxiaoqiang@nudt.edu.cn, ORCID 0000-0001-9476-8026
Color versions of one or more of the figures in this paper are available online.

system materials, problems of radial extrusion and under-constraint of the lens are often generated during temperature change. As a result, the actual thermal deformation of the optical components cannot be performed as intended, or the positioning fails. Thus it is necessary to optimize the lens-assembly structure.

In this paper, the theoretical relationship between the temperature characteristics and the shape and material of the lens is obtained, providing an optimized approach to athermalization of optical systems. At the same time, for the specific requirements of an optical system's temperature adaptability, a new lens-assembly structure is proposed. Combined with the above theoretical model, the optical system can be athermalized, under the condition of ensuring that the radial and axial directions of the lens have no issues about constraint. Finally, to prove the validity of the analysis, we take the improved R-C system as an example and design such a system using the athermal idea. Simulation results show that the imaging quality is good in the temperature range of -60~100°C, so the athermalization requirement is achieved.

II. TEMPERATURE CHARACTERISTICS OF THE FOCUS

The offset of the focus is an essential manifestation of the thermal effect on an optical system. When the offset between the focal plane and actual image plane exceeds the system's focal depth, imaging quality deteriorates sharply. Therefore, thermal defocusing has become a problem that must be solved. First we take the focus as the subject of research, and then we investigate the temperature characteristics of the refractive system.

2.1. Temperature Characteristics of the Focus for a Single Lens

A single lens is shown in Fig. 1. If we consider the medium's refractive index to be a fixed value of 1, the following equation can be obtained from the thin-lens formula:

$$\begin{cases} \dfrac{1}{f'} = \dfrac{(r_2\text{-}r_1)(n-1)}{r_1 r_2} = \varphi \\ l_H' = \dfrac{-r_2 D}{n(r_2 - r_1)} \end{cases}, \tag{1}$$

where φ is the lens power, and n is the refractive index of the lens material. The principal plane of the lens does not coincide with the apex of the optical surface, and the principal plane moves with temperature. Therefore, unlike for a mirror, the displacement of the lens's focus is not characterized by the change in the focal length, but rather by the back focal length l_F'. From Fig. 1 we know that $l_F' = f' + l_H'$, with r_1, r_2, D, and n all functions of temperature. Taking the derivative of l_F' with respect to T, we obtain the following equation:

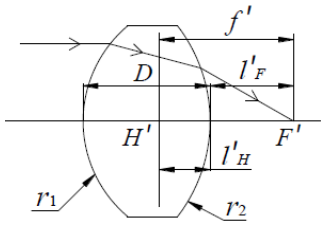

FIG. 1. Temperature characteristics of the focus for a single lens.

$$\frac{dl_F'}{dT} = \frac{df'}{dT} + \frac{dl_H'}{dT} = \frac{r_1 r_2[n\beta - (n-1)\alpha]}{(n-1)^2(r_1 - r_2)} + \frac{r_2(\beta - \alpha)D}{n(r_2 - r_1)}, \tag{2}$$

where α is the thermal expansivity of the lens, and $\beta = dn/ndT$. In Eq. (2), r_1, r_2, and D represent shape information, and n, α, and β represent material information. These six basic design parameters determine the direction and magnitude of change in the back focal length of a single lens under uniform temperature change. Therefore, we have established a mathematical model between the back focal length's temperature characteristics and the lens's shape and its material properties, in Eq. (2).

2.2. Temperature Characteristics of the Focus for a Multilens System

The positive and negative of dl_F'/dT and its absolute value respectively determine the direction and magnitude of motion of a single lens's focus with temperature change. Based on the above analysis, if we find the relationship between dl_F'/dT and the design parameters, we can obtain a temperature-dependent model for an optical system.

For the refractive multilens system shown in Fig. 2, the total power φ can be found as follows:

$$\varphi = \frac{1}{h_1}\sum_{i=1}^{k} h_i \varphi_i, \tag{3}$$

where k represents the number of lenses, h_i represents the height of the first paraxial ray at each lens, and φ_i

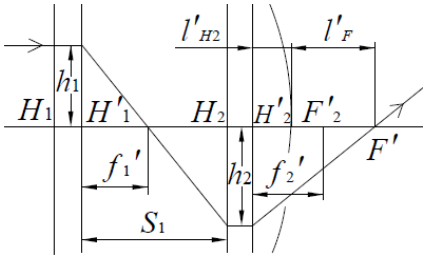

FIG. 2. Temperature characteristics of the focus for a multilens system.

represents the focal power of the $i^{'}$th lens. At the same time, the change in back focal length is $\Delta l_F^{'} = -(\frac{1}{h_1\varphi})^2 \sum_{i=1}^{k}(h_i^2 \Delta\varphi_i)$ [12]. If $h_1 = 1$, by taking the derivative of $l_F^{'}$ with respect to T we get the following equation:

$$\frac{dl_F^{'}}{dT} = -\sum_{i=1}^{k}[(h_i^2 \frac{d\varphi_i}{\varphi_i dT}\varphi_i)/\varphi^2]. \quad (4)$$

Equations (3) and (4) are the classic formulas for focal power and thermal aberration. It can be seen that there is coupling between h_i and the design parameters in the two equations, so it is difficult to calculate the specific parameters of the system from these two equations. Most reports have used only these two formulas to introduce the principle of athermalization. However, this formula contains shape and material information about the lens. Replacing focal powerwith focal length in Eq. (4), we obtain the following equation:

$$\frac{dl_F^{'}}{dT} = \sum_{i=1}^{k}[(h_i^2 \frac{df_i^{'}}{dT}(\frac{f^{'}}{f_i^{'}})^2]. \quad (5)$$

We can establish a mathematical model between the basic design parameters such as r_i, S_i, D_i, n_i, α_i and β_i and the temperature characteristics of the focus through intermediate quantities such as h_i, $f_i^{'}$ and $f^{'}$.

In Eq. (5), only $df_i^{'}/dT$ determines the positive or negative sign of each item $h_i^2 \frac{df_i^{'}}{dT}(\frac{f^{'}}{f_i^{'}})^2$. At the same time, we can find $\frac{df_i^{'}}{dT} = \frac{r_{i1}\,r_{i2}[\beta_i n_i - \alpha_i(n_i-1)]}{(n_i-1)^2(r_{i1}-r_{i2})}$ from Eq. (2), where the positive and negative characters of r_{i1}, r_{i2} and $(r_{i1}-r_{i2})$ determine just the shape of the lens, and α_i and β_i are the material properties of the lens under temperature change. When the lens material is selected, the positive and negative sign and even the specific value of each $[\beta_i n_i - \alpha_i(n_i-1)]$ has been determined. It is known from Eq. (1) that $f_i^{'} = \frac{r_{i1}r_{i2}}{(n_i-1)(r_{i2}-r_{i1})}$, and the positive and negative character of Eq. (1) is only related to the shape of the lens. Therefore, according to the characteristics of the formulas above, we can obtain the relationship between the focus's temperature characteristics and the shape and material of the lens. The shape and material information of the lens is the set of parameters that we need to determine when designing an optical system.

Now we summarize the relationships above. Design rules are shown in Table 1.

In the case of $[\beta_i n_i - \alpha_i(n_i-1)] > 0$, the positive and negative character of $h_i^2 \frac{df_i^{'}}{dT}(\frac{f^{'}}{f_i^{'}})^2$ is simply the opposite of that shown in Table 1.

TABLE 1. Thermal characteristics based on lens shape and displacement of focus, and focal length

$[\beta_i n_i - \alpha_i(n_i-1)]$	r_{i1}	r_{i2}	$r_{i1}-r_{i2}$	Shape	$h_i^2 \frac{df_i^{'}}{dT}(\frac{f^{'}}{f_i^{'}})^2$	$f_i^{'}$
<0	>0	>0	>0		<0	<0
	<0	<0	>0			
	<0	>0	<0			
	>0	>0	<0		>0	>0
	<0	<0	<0			
	>0	<0	>0			

Since $\Delta l_F^{'} = (dl_F^{'}/dT)\,\Delta T$, the positive and negative character of $dl_F^{'}/dT$ and ΔT can be used to judge the movement trend of the focus. For example, if $\frac{dl_F^{'}}{dT} > 0$ and $\Delta T > 0$, under the direction rule of "left is negative and right is positive", the focus $F^{'}$ always moves to the right along the optical axis, and the amount of movement is proportional to the value of $|\frac{dl_F^{'}}{dT}|$. As shown in Eq. (5), $\frac{dl_F^{'}}{dT} = \sum_{i=1}^{k} E_i$, so there is only an additive relationship between $dl_F^{'}/dT$ and E_i. For optical design, the relationship between the back focal length's temperature characteristics and the shape and material of the lens in Table 1 can help researchers determine and correct the focus's position and mobility trend under temperature change, at various stages of optical design. The designer can ascertain the value of $[\beta_i n_i - \alpha_i(n_i-1)]$ by selecting the material first, and then find the correct initial optimization direction by choosing the shape of the lens. Through the above method, thermal analysis and optimization of the optical system can be performed quickly. This method can especially improve the efficiency of using software to design an optical system for athermalization. While optical design relies heavily on software, if it lacks the correct initial optimization direction, the design process will take a long time. Therefore, when a designer uses software to develop an athermal design, this method can greatly improve efficiency.

There is no chromatic aberration in a reflective system, but a refractive system does feature it. Therefore, to maintain good temperature characteristics for a refractive system, it is necessary to eliminate not only thermal but also chromatic aberration. A refractive system, especially an infrared one, mainly eliminates chromatic aberration by matching the chromatic aberration coefficients C_i of the optical materials [13], and should satisfy the following equation:

$$\sum_{i=1}^{k}[(h_i^2 C_i\varphi_i)/(h_1\varphi)^2] = 0 . \quad (6)$$

Equation (6), combined with the focal-power and thermal-aberration formulas, constitute a relatively complete theory of athermalization.

III. INTRODUCTION OF NEW ASSEMBLY STRUCTURE

The above analysis provides the theoretical gist of athermalization design of an optical system. However, if the optical system so optimized cannot reproduce the optimized results for an actual instrument, we still cannot design the optical instrument using athermalization.

3.1. Analysis of a Traditional Assembly Structure

At present, both theoretical calculations and software design are performed by placing optical components in an unconstrained state. However, in an actual optomechanical system, due to the differences in thermal expansivity between components, conditions are often overconstrained or underconstrained during temperature change. Axial constraint problems can be absolutely eliminated by a combination of spacers of different expansivity, but, due to the need for positioning, there is inevitably a radial constraint problem in the common assembly structure of a lens, shown in Fig. 3. Therefore, how to make the actual optical components yield thermal deformation according to the expected thermal behavior, and thus how to reproduce the expected system performance in the actual system, becomes an urgent problem to be solved.

As shown in Fig. 3, we assume that the half height of the lens is m, the inner radius of the drawtube is q, the thermal expansivity of the lens is α_m, and the thermal expansivity of the drawtube is α_q. At the designed temperature, $m = q$ is generally required to ensure assembly accuracy. If $\alpha_m < \alpha_q$ and $\Delta T > 0$, when the value of uniform temperature change is ΔT, then the upper and lower end faces of the lens will separate from the inner wall of the drawtube. This situation will cause the lens to be underconstrained, and eventually will lead to positioning failure. If $\Delta T < 0$, the lens will be squeezed by the drawtube, resulting in the lens's actual thermal deformation being different from the result from analysis. This situation will cause the image quality to deteriorate, and could even damage the lens.

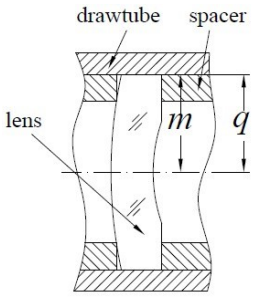

FIG. 3. The traditional structure of a lens assembly.

3.2. Proposal and Parameter Calculation for the New Assembly Structure

Considering the above problems, we propose a new assembly structure, as shown in Fig. 4.

Comparing to Fig. 3, we can find that the new assembly structure changes the lens's end face 1 to a bevel, instead of the natural extension of the original optical surface, with a slope angle θ.

We first analyze the angular change of the lens's end face 1 and the corresponding drawtube's bevel during thermal deformation, that is, the change of θ. As shown in Fig. 5, $\tan\theta = \dfrac{m-j}{a}$ for end face 1, so that when the structure undergoes a uniform temperature change ΔT the following equation is obtained:

$$\tan\theta' = \frac{(m-j)(1+\alpha_m \Delta T)}{a(1+\alpha_m \Delta T)} = \tan\theta . \quad (7)$$

From Eq. (7) we can see that the temperature characteristic of the angle is independent of the thermal expansivity, so the angle does not change with temperature.

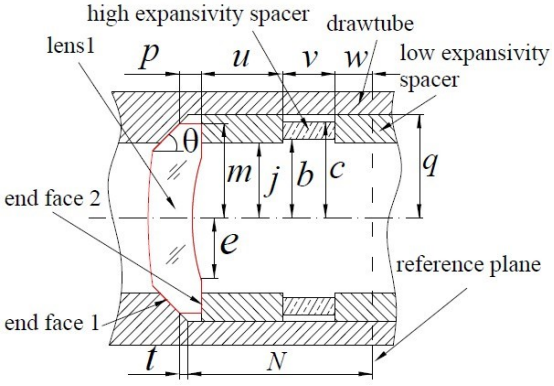

FIG. 4. The new assembly structure for the lens.

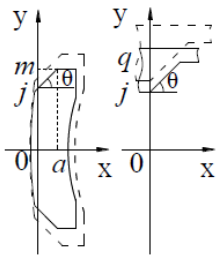

FIG. 5. Temperature characteristic of the end face's slope angle.

It is not difficult to prove that $\tan\theta' = \tan\theta$ for the bevel of the drawtube. In summary, we conclude that the bevel does not change during thermal deformation. Therefore, end face 1 of the lens and the corresponding bevel of the drawtube will always maintain surface contact during uniform temperature change.

Assuming that the operating temperature range of the system is $\pm\Delta T_{\max}$, we notice that the upper and lower end faces of the lens in Fig. 4 are not in contact with the inner wall of the drawtube, wherein the lens's half height m and the inner radius q of the drawtube should satisfy the following inequality:

$$\begin{cases} m - m\alpha_m \Delta T_{\max} \le q - q\alpha_q \Delta T_{\max} \\ m + m\alpha_m \Delta T_{\max} \ge j + j\alpha_q \Delta T_{\max} \end{cases}. \tag{8}$$

The assembly structure must satisfy Inequality (8) to ensure that the lens is not squeezed radially by the drawtube at the lowest operating temperature, and does not lose its self-positioning function at the highest operating temperature. The positioning accuracy of the lens is mainly ensured by cooperation between the lens's end face 1 and the drawtube's corresponding bevel. When the temperature changes, the two bevels slide relative to each other; therefore, to ensure self-positioning of the tapered structure, it is required that the lens should always be in contact with the corresponding bevel of the drawtube. As shown in Fig. 4, we introduce a high-expansivity spacer with thermal expansivity α_c. The axial length of this spacer is v, and its outer radius c should satisfy the following inequality:

$$\begin{cases} c - c\alpha_c \Delta T_{\max} \ge j - j\alpha_q \Delta T_{\max} \\ c + c\alpha_c \Delta T_{\max} \le q + q\alpha_q \Delta T_{\max} \end{cases}. \tag{9}$$

If the assembly structure satisfies Inequality (9), it guarantees that the spacer will not lose its spacing effect at the lowest operating temperature, and will not radially compress the inner wall of the drawtube at the highest operating temperature. At the same time, its inner radius b should not be too small, to avoid blocking the light path.

Next, based on the reference surface, we analyze the conditions that make the axial thermal deformation of the drawtube and the corresponding components consistent during temperature change. At the design temperature, the assembly structure satisfies the following equation:

$$N + t = p + u + v + w. \tag{10}$$

Equation (10) guarantees the positioning accuracy of the lens. When the system experiences a uniform temperature change ΔT, the following equation must be satisfied:

$$N' + t' = p' + u' + v' + w', \tag{11}$$

where $N' = N + N\alpha_q \Delta T$, $p' = p + p\alpha_m \Delta T$, $u' = u + u\alpha_q \Delta T$, and $v' = v + v\alpha_c \Delta T$. Since end face 1 of the lens and the corresponding bevel of the drawtube slide relatively, the inequality $t' \ne t + t\alpha_q \Delta T$ is established. We can obtain the equation $t = \dfrac{q-m}{\tan\theta}$ from the geometric relationship; therefore, the length t satisfies Eq. (12):

$$t' = \frac{q' - m'}{\tan\theta} = \frac{q + q\alpha_q \Delta T - (m + m\alpha_m \Delta T)}{\tan\theta}. \tag{12}$$

Thus Eq. (11) can be simplified to Eq. (13):

$$N\alpha_q + q\alpha_q / \tan\theta - m\alpha_m / \tan\theta = p\alpha_m + u\alpha_q + v\alpha_c + w\alpha_q. \tag{13}$$

Equation (13) is only related to material information and is independent of temperature, which indicates that the assembly structure meets the requirements for positioning accuracy under uniform temperature change. At the same time, Eqs. (10) and (13) can determine two variables, indicating that the values of the remaining parameters in the two equations can be defined according to specific requirements. Meanwhile, there are no strict requirements for radial size or accuracy for the high-expansivity spacer, as long as Inequality (9) is satisfied.

3.3. Extension and Summary of the New Assembly Structure

Meanwhile, if the lens and spacer are in different positions, the lens will have different displacement effects relative to the drawtube during temperature change. For example, if we change the assembly structure shown in Fig. 4 to that in Fig. 6, because the contact surface between lens and drawtube is now a vertical plane, there is no axial slip between them during thermal deformation. Hence, we can control the direction and amount of slippage of the lens during temperature change by properly arranging the relative positions of the high- and low-expansivity spacers, lens, and drawtube, and selecting the appropriate slope angle of the end face. Finally, the slip effect is consistent with the expected design results. The calculation

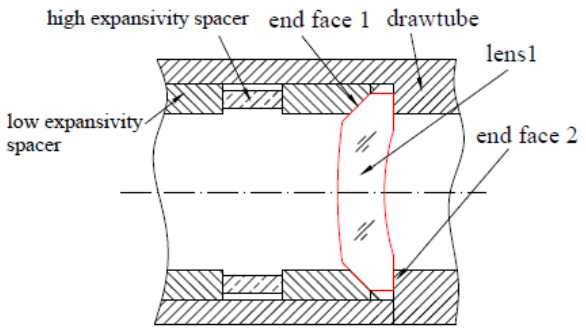

FIG. 6. Adjustment diagram of the new assembly structure.

of its structural parameters is similar for different layouts of lens and spacer.

More generally, any of the above structures consisting of a number of lenses and spacers should be guaranteed to satisfy the following equation:

$$\sum\Delta_S+\sum\Delta_L+\sum\Delta_P=\sum\Delta_B\,, \tag{14}$$

where $\sum\Delta_S$ represents the total thermal deformation of all spacers in the axial direction, $\sum\Delta_L$ represents the total thermal deformation of all lenses in the axial direction, $\sum\Delta_P$ represents the total slippage of all lenses in the axial direction, and $\sum\Delta_B$ represents the total thermal deformation of the corresponding drawtubes in the axial direction. The calculation of each variable in Eq. (14) is similar to that for the structure above. The assembly structure above converts the radial displacement of the lens (relative to the drawtube) into an axial sliding, and solves the problem of radial constraint of the lens during the temperature change, on the basis of ensuring that the self-positioning function works. However, to prevent the self-locking phenomenon caused by excessive friction, the slant angle θ should not be too small. At the same time, to ensure the positioning function, the slant angle θ should not be too large. We find that the new assembly structure solves the axial constraint and positioning problems of the lens while also solving its radial constraint and positioning problems. It can also be used to control the axial position of the lens during temperature change.

IV. DESIGN EXAMPLE AND DISCUSSION

By introducing the focus's temperature characteristics and the new assembly structure, a relatively complete design method for the athermalization of an optical system has been achieved. As shown in Fig. 7, taking the catadioptric system ($F=6.67$) as an example, a specific application is used to verify the above conclusions; then the general rules are summarized.

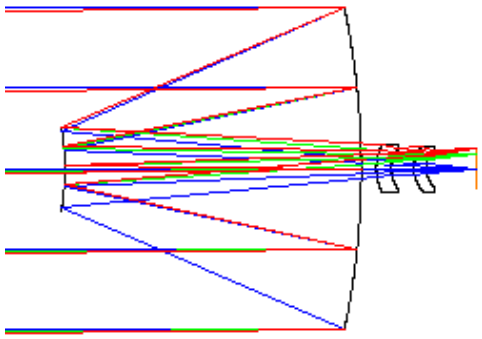

FIG. 7. The optical principle of a catadioptric system.

4.1. Verification and Application of the Temperature Characteristics of the Focus

The design parameters of the catadioptric system are shown in Table 2.

The catadioptric system shown in Fig. 7 is divided into reflection and refraction systems for analysis. In the reflection system (R-C system), the material of the integrated mirror and drawtube is AL6061 ($TCE=23\times10^{-6}/℃$). The 'FOLLOW' command in the Zemax software package is used to assign material properties to the reflector. After setting the thermal expansivity of air in the intervals in the mirror group, three typical temperatures of -60, 20, and 100°C were established prior to thermal analysis and system optimization. As shown in Fig. 8, the back focal length of the R-C system changes linearly, and the ratio of the slope to the original back focal length (190.5032 mm) is equal to the material's thermal expansivity. Therefore, if the image plane overlapped with the focal plane at 20°C, the focal plane would overlap with the image plane throughout the temperature range, verifying the conclusion mentioned in the introduction that there is no thermal aberration in a homogeneous-material reflection system.

Due to the short back focal length of the R-C system, which is not conducive to installing subsequent components, the lens group should be able to extend the back focal length. It can be found from Table 1 that four lens shapes with negative optical power meet the requirements of focal power to achieve the effect of extended back focal length. To explain the formula laws clearly and eliminate the effect of formula coupling, we adopt the shapes of the two lensesfrom the first row of Table 1, as shown in Fig. 7. Since the lens is made of K9 glass, the material properties satisfy the inequality $[\beta n-\alpha(n-1)]<0$, so $h_1^{\,2}\frac{df_1'}{dT}(\frac{f'}{f_1'})^2<0$

TABLE 2. Design parameters of the catadioptric system

Wavelength	0.486~0.656 μm
F number	6.7
FOV	0.74° × 1°
EFL	1000 mm
BFL	22.76 mm

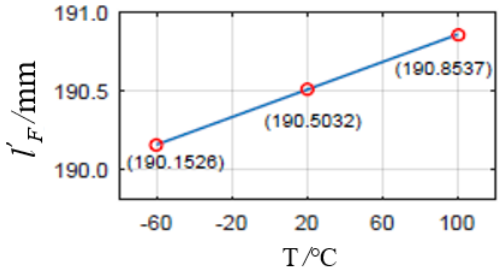

FIG. 8. The change in back focal length of the R-C system.

and $h_2^2 \frac{df_2'}{dT}(\frac{f'}{f_2'})^2 < 0$. After the distribution of the focal power in the system, the thermal expansivity of the air gap is set to be the same as that of the reflection system, and the temperature configuration is established. The size of the spot diagram is chosen as the optimization target.

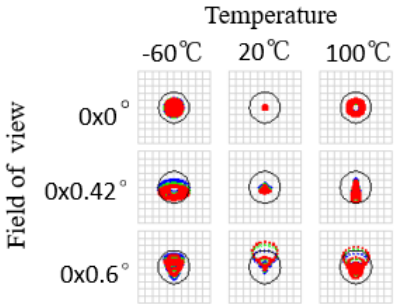

FIG. 9. The spot diagrams for the catadioptric system.

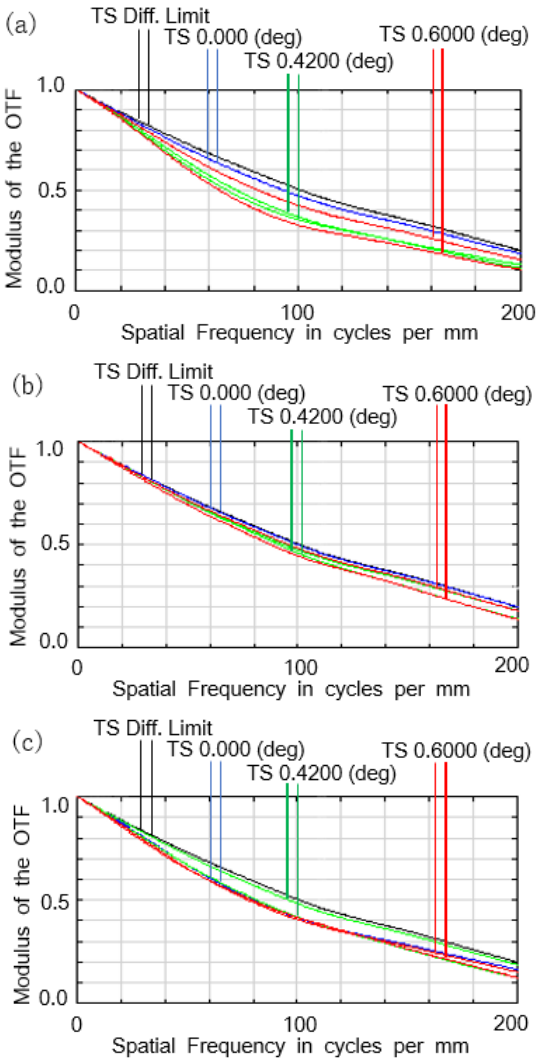

FIG. 10. The transfer functions of the catadioptric system: (a) -60°C, (b)20°C, and (c) 100°C.

After optimization, the catadioptric system in Fig. 7 is obtained. The results for the spot diagram's size and MTF for each temperature are shown in Figs. 9 and 10.

It can be seen from Fig. 9 that the spot diagrams of the system are basically within Airy speckle for each configuration of field of view and temperature (where the Airy radius is 4.275 μm). The MTF of the system at each temperature is greater than 0.1 at 200 lp/mm, per Fig. 10. Thus the system has good temperature adaptability.

Next the temperature characteristics of the refraction system in the catadioptric setup are analyzed separately. The thermal expansivity of the air spacing between the two lenses is kept unchanged, and the changes of focal length at various temperatures are shown in Fig. 11.

It can be seen from Fig. 11 that the focus of the refraction system moves to the left and away from the final optical surface with increasing temperature, which is consistent with the conclusion in Table 1 and proves the correctness of the theoretical model.

4.2. Verification of Assembly Structure

The effect of temperature change on the imaging quality of an actual optomechanical system can be found by software simulation. To reduce the error caused by simulating a complex structure, to obtain the direct impact, and to facilitate reproduction of this work by readers, the first lens of the above catadioptric system is analyzed separately.

According to design experience and calculation results, the structural parameters shown in Table 3 are chosen for modeling.

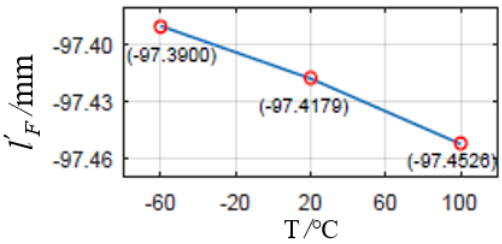

FIG. 11. The change in back focal length of the refraction system.

TABLE 3. Parameters of the new assembly structure

Variable	Value/mm	Variable	Value/mm
m	14.000000	v	5.635130
j	12.000000	w	5.000000
b	12.500000	N	26.283805
c	14.500000	t	1.732051
q	15.000000	r_1	23.977862
e	10.000000	r_2	15.690418
p	3.916624	D	7.000000
u	10.000000		

AL6061 is selected as the material of the drawtube, the integrated mirrors, and the low-expansivity spacer. Teflon is used for the high-expansivity spacer, and the lens material is K9 glass ($\alpha_q = 23\times10^{-6}$ /℃, $\alpha_c = 110\times10^{-6}$ /℃, $\alpha_m = 7.5\times10^{-6}$ /℃). According to the characteristics of the lens structure, the value of the angle θ is 30°, and the wall thickness of the drawtube is 5 mm. These values satisfy Eq. (10) and Fig. 11.

Because the main subject of this research is the radial extrusion of the lens, simulation at the lowest operating temperature of -60°C should be performed. Results of simulations using the Ansys Workbench software, for the traditional and new assembly structures, are shown in Figs. 12~15. In Fig. 12 the radial deformation of the lens in the traditional assembly structure is 0.053576 mm, due to radial extrusion of the lens barrel, which is far greater than the expected thermal deformation of 0.016800 mm in the unconstrained state, and thus has a relatively obvious impact on the shape of the lens's optical surface. In contrast, in the new assembly sufficient gaps are left between upper and lower ends of the lens and the inner wall of the drawtube, so that the lens will not be radially squeezed by the drawtube. As can be seen from Fig. 13, the total radial deformation of the lens is 0.016224 mm, which is basically the same as the expected thermal deformation in the unconstrained state. In the simulation, the lens, tube, and each spacer are set to be the contact type that cannot be separated in the axial direction. As shown in Fig. 14, the axial thermal deformation of the Teflon spacer is 0.049458 mm, which is consistent with the theoretical axial deformation of 0.049589 mm in the unconstrained state. In Fig. 15, the axial uniform-deformation ring also shows that the new assembly does not produce constrained deformation, ensuring the accuracy of axial positioning.

For comparison, the imaging quality of the conventional assembly system at -60°C is shown in Figs. 16 and 17. The results show that the spot diagram (Airy radius 4.264 μm) and MTF of the catadioptric system in the traditional assembly structure are worse than those in Figs. 9 and 10(a), indicating that constrained deformation of a lens has a significant impact on imaging quality. In conclusion, this proves the effectiveness and necessity of the new assembly structure described in this paper.

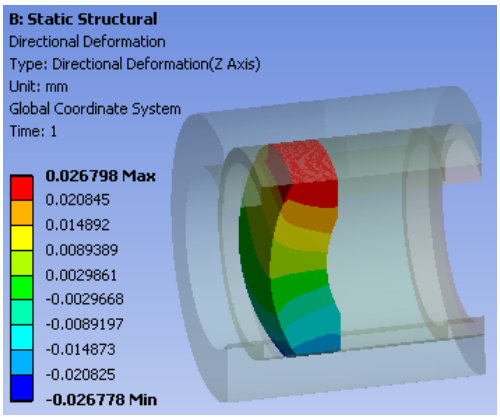

FIG. 12. Radial deformation of the lens in the traditional assembly structure.

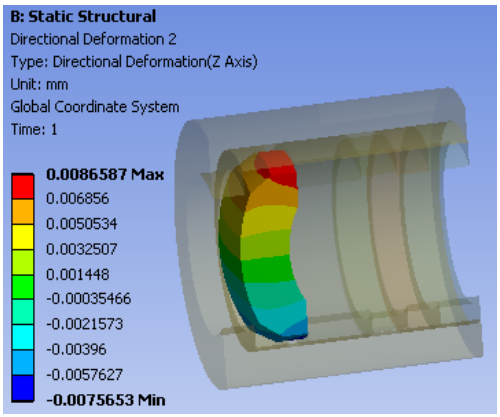

FIG. 13. Radial deformation of the lens in the new assembly structure.

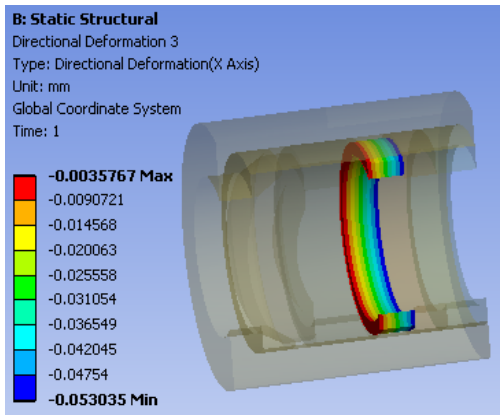

FIG. 14. Axial deformation of the Teflon spacer.

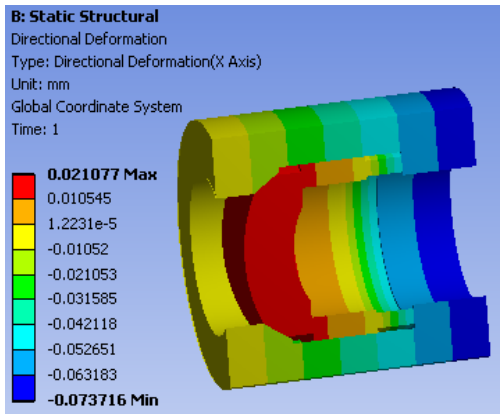

FIG. 15. Axial deformation of the new assembly structure.

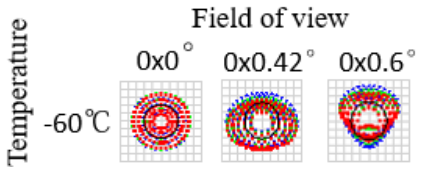

FIG. 16. The spot diagram for the catadioptric system at -60°C.

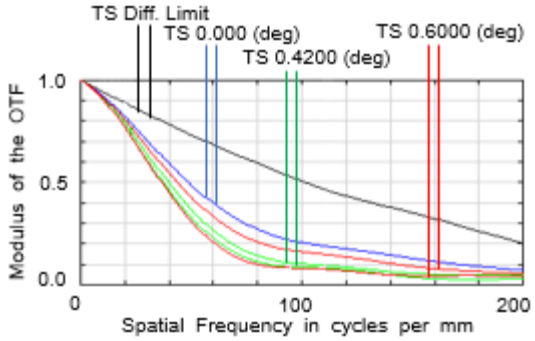

FIG. 17. The transfer functions of the catadioptric system at -60°C.

When the second lens also adopts the new assembly structure, its thermal deformation will be consistent with the expected theoretical analysis, and the main and secondary mirrors of the improved R-C system meet the conditions of a homogeneous-material reflection system. Therefore, the actual thermal performance of the entire optical system will be consistent with the expected effect at the design stage. It can be proved that the improved R-C system will have good imaging quality, as shown in Figs. 9 and 10, over the temperature range from -60 to 100°C.

V. CONCLUSION

Athermal design is a necessary method to improve the temperature adaptability of an optical system. In this paper the relationships between the temperature characteristics of an optical system and lens material and shape are obtained, and the corresponding rules are summarized in detail. In the example, the change of the back focal length of the refractive system under changing temperature is consistent with the theoretical analysis, which verifies the correctness of the theoretical model. Further considering the athermal design requirements of the system for fabrication, a new assembly structure of the lens is proposed. This assembly structure enables the lens to generate no constraining stress during uniform temperature change, which ensures positioning accuracy. Therefore, the assembly structure not only solves the constraint and positioning problems caused by the difference in thermal expansivity between lens and drawtube, but also ensures the athermalization of the actual optical system. Adopting this athermal design method and new assembly structure, the chosen optical system can achieve the design requirements of athermalization. The athermal method and assembly structure are also applicable to other optical systems, so they have a certain practicability and universality, and can provide a reference for improving the environmental adaptability of optical systems.

ACKNOWLEDGMENT

This research was supported by the Science Challenge Project (TZ2018006) and the Key Program of the National Natural Science Foundation of China (No. 51835013). The authors thank Jianpeng Wang for valuable discussions.

REFERENCES

1. L. W. Yang, Z. L. Li, H. W. Xin, H. Xu, and Y. C. Fan, "Design and analysis for structure of small infrared camera," Infrared Laser Eng. **44**, 3025-3031 (2015).
2. J. Gao, "Athermalizing optical system design of airborne navigation infrared lmage," M. S. *Thesis*, Xi'an: Xi'an Technological University (2013).
3. D. Vukobratovich and J. P. Schaefer, "Large stable aluminum optics for aerospace applications," Proc. SPIE **8125**, 21250T (2011).
4. J. Dong, Y. Zhang, and S. Chen, "Optical design and athermalization analysis of infrared dual band refractive-diffractive telephoto objective," Proc. SPIE **10250**, 102500H (2017).
5. R. Y. Li, Y. G. Fu, and Z. Y. Liu, "Athermalization design of compact medium-wave infrared imaging system," Infrared Technol. **40**, 119-124 (2018).
6. D. Kucukcelebi, "Optical design of an athermalised dual field of view step zoom optical system in MWIR," Proc. SPIE **10375**, 103750S (2017).
7. M. D. Shen and H. H. Ren, "Design of a wide temperature dual spectrum infrared search and tracking system," Acta Phys. Sin. **62**, 090702 (2013).
8. J. Liu and T. Li, "Athermal design of a compact MWIR dual field-of-view optical system," Proc. SPIE **10846**, 1084618 (2018).
9. N. Xie, Q. F. Cui, L. Sun, and J. F. Wang, "Optical athermalization in the visible waveband using the 1+Σ method," Appl. Opt. **58**, 635-641 (2019).
10. X. X. Wang and M. Y. Jiao, "Athermalization design for infrared optical systems," J. Appl. Opt. **30**, 129-133 (2009).
11. C. Y. Chan, T. M. Huang, and P. W. Hwang, "Development of an athermalized optomechanical system of large aperture remote sensing instruments," Proc. SPIE **10371**, 103710U (2017).
12. Y. Tamagawa and T. Tajime, "Expansion of an athermal chart into a multilens system with thick lenses spaced apart," Opt. Eng. **35**, 3001-3006 (1996).
13. B. I. Ahn, Y. S. Kim, and S. C. Park, "Athermal and achromatic design for a night vision camera using tolerable housing boundary on an expanded athermal glass map," Curr. Opt. Photon. **1**, 125-131 (2017).